Environmental Science Nano

Bottom-Up Biofilm Eradication Using Bacteriophage-Loaded Magnetic Nanocomposites: A Computational and Experimental Study

Journal:	*Environmental Science: Nano*
Manuscript ID	EN-ART-07-2019-000827.R1
Article Type:	Paper
Date Submitted by the Author:	04-Sep-2019
Complete List of Authors:	Yu, Pingfeng; Rice University, Civil and Environmental Engineering Wang, Zijian; Rice University, Civil and Environmental Engineering Marcos-Hernandez, Mariana; University of Texas at El Paso, Chemistry and Biochemistry Zhang, Danning; Rice University, Civil and Environmental Engineering Zuo, Pengxiao; Rice University, Civil and Environmental Engineering Powell, Camilah; Rice University, Chemical and Biomolecular Engineering Pan, Aaron; Rice University, Chemical and Biomolecular Engineering Villagran, Dino; University of Texas at El Paso, Chemistry and Biochemistry Wong, Michael; Rice University, Chemical and Biomolecular Engineering Alvarez, Pedro; Rice University, Civil and Environmental Engineering

ENVIRONMENTAL SIGNIFICANCE

Biofilms, which are very difficult to eradicate from water treatment, distribution and reuse systems, can cause a variety of safety, aesthetic and corrosion problems. This underscores the need for effective and sustainable biofilm-eradication technologies. Here, we covalently loaded bacteriophages with optimized phage orientation onto Fe_3O_4-based magnetic nanocomposites. Pushed by a weak magnetic field, phage-nanocomposite conjugates (PNCs) targeted the dominant species at the base of the biofilm and de-anchored it within six hours. This combined experimental and computational study revealed that smaller PNCs enhanced biofilm bottom clearance with significant horizontal dispersion, while larger PNCs exerted more significant vertical biofilm disruption. Our study highlights the role of PNC size on biofilm eradication patterns and advances the scientific basis for nanotechnology-enhanced, phage-based strategies for biofilm control. Potential applications include membrane biofouling control and biocorrosion mitigation.

Bottom-Up Biofilm Eradication Using Bacteriophage-Loaded Magnetic Nanocomposites: A Computational and Experimental Study

Pingfeng Yu [1, 2, *], Zijian Wang [2], Mariana Marcos-Hernandez [1, 3], Pengxiao Zuo [2], Danning Zhang [1, 2], Camilah Powell [1, 4], Aaron Y. Pan [2], Dino Villagrán [1, 3], Michael S. Wong [1, 2, 4], and Pedro J.J. Alvarez[1, 2, 4 *]

[1]Nanosystems Engineering Research Center for Nanotechnology-Enabled Water Treatment.

[2]Department of Civil and Environmental Engineering, Rice University, Houston, Texas, USA

[3]Department of Chemistry and Biochemistry, The University of Texas at El Paso, El Paso, USA

[4]Department of Chemical and Biomolecular Engineering, Rice University, Houston, Texas, USA

*Corresponding authors: pingfeng.yu@rice.edu (P. Yu); alvarez@rice.edu (P. Alvarez).

ABSTRACT

Biofilms cause a variety of pervasive problems in water treatment, distribution and reuse systems that are difficult to mitigate due to their resistance to disinfectants. We used magnetic phage-nanocomposite conjugates (PNCs) to target bacteria in biofilm inner layers for bottom-up eradication. Polyvalent *Podoviridae* phages PEB1 (54 nm) or PEB2 (86 nm) were covalently conjugated (via amide bonds) with magnetic colloidal nanoparticle clusters (CNCs) of different sizes (150, 250 or 500 nm). Smaller CNCs with higher density of amino groups loaded phages more efficiently than the largest CNCs (e.g., for PEB1, 60±4, 62±5, and 47±4 phages were loaded per μm^2). Smaller PNCs dispersed phages more evenly throughout the biofilm bottom, significantly disrupting the biofilm bottom layer and detaching the biofilm within 6 h. The biofilm removal efficiency was 98.3±1.4 % for dual species biofilm (i.e., *Escherichia coli* and *Pseudomonas aeruginosa*) and 92.2±3.1 % for multi-species biofilm (i.e., *E. coli*, *P. aeruginosa*, and non-hosts *Bacillus subtilis* and *Shewanella oneidensis*). Large PNCs caused higher physical disruption but lower corresponding removal efficiencies (i.e., 80.2±3.4 % for dual species biofilm and 67.6±3.8 % for multi-species biofilm) due to lower horizontal diffusion at the bottom of the biofilm. A semi-empirical numerical model corroborated the higher biofilm removal efficiency with smaller PNCs and inferred that PNC size influences the mode of phage propagation: Small PNCs facilitate biofilm bottom clearance with significant horizontal dispersion while large PNCs mainly enhance vertical propagation. Overall, this study demonstrates the importance of size control to enhance the biofilm eradication capability of PNCs as an alternative or complementary biofilm control strategy.

ENVIRONMENTAL SIGNIFICANCE

Biofilms, which are very difficult to eradicate from water treatment, distribution and reuse systems, can cause a variety of safety, aesthetic and corrosion problems. This underscores the need for effective and sustainable biofilm-eradication technologies. Here, we covalently loaded bacteriophages with optimized phage orientation onto Fe_3O_4-based magnetic nanocomposites. Pushed by a weak magnetic field, phage-nanocomposite conjugates (PNCs) targeted the dominant species at the base of the biofilm and de-anchored it within six hours. This combined experimental and computational study revealed that smaller PNCs enhanced biofilm bottom clearance with significant horizontal dispersion, while larger PNCs exerted more significant vertical biofilm disruption. Our study highlights the role of PNC size on biofilm eradication patterns and advances the scientific basis for nanotechnology-enhanced, phage-based strategies for biofilm control. Potential applications include membrane biofouling control and biocorrosion mitigation.

INTRODUCTION

Biofilms, which are microbial communities that attach to surfaces, are a pervasive problem in water supply systems due to their potential to increase significantly the cost and complexity of water treatment and distribution. For example, biofilms can deteriorate treatment process performance (e.g., membrane biofouling), [1] impart taste and odor, [2] harbor pathogens, [3, 4] and accelerate water infrastructure corrosion. [5] Biofilms are resistant to conventional chemical disinfectants that do not easily penetrate the extracellular polymeric substrates (EPS) matrix, [6] which is exacerbated by the development of bacterial resistance to disinfectants.[7] Therefore, there is a critical need to develop alternative and complementary biofilm eradication methods that are robust and sustainable to improve water treatment and distribution system resiliency.

Phages are viruses that exclusively infect bacteria, making them generally harmless to humans and safe to use for microbial control in water systems.[8] As the most diverse and abundant living entities on the planet,[9] some phages possess very useful traits for biofilm eradication, such as broad host range (i.e., polyvalence) and polysaccharide depolymerase production to break down the biofilm EPS matrix.[10, 11] Recent advances in phage ecology and genomics have facilitated isolation and production of such phages.[11, 12] Furthermore, appropriate phages can be immobilized onto superparamagnetic nanocomposites (by chemical binding[13, 14]) and delivered directly to the relatively inaccessibe inner layer of the biofilm with the help of low-energy magnetic fields.[15] Covalent conjugation between the carboxyl group on phage head and amino groups on nanocomposites via amide bonds ensures right phage orientation (i.e., tail fibers exposed for bacterial recognition and attachment) on the phage-nanocomposites

conjugates (PNCs).[14, 15] Such PNCs may open new avenues to de-anchor biofilms in water systems and mitigate related economic and health concerns.

Biofilm eradication by PNCs hinges on phage propagation dynamics, which depends on PNC size (influencing biofilm penetration potential and physical disruption capability) and the number of phages that can be loaded on magnetic particles (each PNC represents a potential infectious center,[16, 17] but more phages on the PNC increase the probability of successful infection[18, 19]). Ideally, PNCs should penetrate easily and disrupt biofilm significantly while minimizing aggregation to enhance phage propagation. However, it is unknown how nanocomposite and phage sizes affect biofilm penetration and removal efficiency, which is a critical knowledge gap for effective PNC application.

Computational models are useful tools to study bacteria-phage interactions and phage propagation in biofilms[16, 18-22]. Several stochastic spatial models using experimentally-determined bacteria and phage parameters (e.g., phage infection rate, diffusion rate and phage trapping/degradation rate) adequately explained the coexistence of bacteria and phages in natural biofilms and showed that biofilm disruption was primarily determined by phage infection and diffusion rates.[18, 20] Such semi-empirical models could be useful to simulate phage proliferation and biofilm removal efficiency by PNCs, which would require consideration of how PNC properties (e.g., phage loading and size) and biofilm physical disruption influence the spatial and temporal patterns of phage propagation.

We coupled our multiple-host (polyvalent) phage isolation approach[23] with biofilm diffusion assays[24] to obtain phages with high biofilm disruption potential. Phages of different sizes were

loaded onto magnetic colloidal nanoparticle clusters (CNCs) of different sizes to optimize biofilm removal. A semi-empirical stochastic spatial model was modified to consider the effects of PNC size on phage diffusion and trapping rates in biofilms. This semi-empirical model corroborated the high biofilm removal efficiency observed experimentally and inferred distinct dynamics of phage propagation by different sized PNCs. This unprecedented computational and experimental study seeks to inform the design and application of this novel PNC-based biofilm control approach.

MATERIALS AND METHODS

Bacteria and cultures. The strains used include *E. coli* NDM-1 (ATCC BAA-2452), *P. aeruginosa* PA01 (ATCC 15692), *Bacillus subtilis* 168 (ATCC 23857), and *Shewanella oneidensis* MR-1 (ATCC 700550). *E. coli* NDM-1 represents an enteric pathogenic bacterium with multidrug resistance.[25] *P. aeruginosa* is an opportunistic pathogen commonly active in biofilm formation.[26] *B. subtilis* and *S. oneidensis* are relatively benign bacteria widely distributed in the environment.[27, 28] These bacteria were initially cultured in Tryptic soy broth (TSB) medium overnight and then transferred to modified M63 medium [2.4 g of KH_2PO_4, 5.6 g of K_2HPO_4, 1.6 g of $(NH_4)_2SO_4$, 0.3 mg $FeSO_4$ per liter water supplemented with 1 mM of $MgSO_4$, 0.2% glucose and 0.5% Casamino Acids] for biofilm formation in microtiter plates (Grace Bio-Labs, Bend, OR) and in a Center for Disease Control (CDC) biofilm reactor (Bioscience, Bozeman, MT) with polypropylene coupons. Total viable bacteria were counted by plate assay using Difco standard bacterial count agar (BD, Sparks, MD) and expressed as colony-forming-units (CFU). *B. subtilis* was enumerated on phenol red polymyxin selective

medium for gram-positive bacteria (HIMEDIA, Mumbai, India), *E. coli* NDM-1 was enumerated on eosin methylene blue (EMB) selective agar (CRITERION, Santa Maria, CA) with 0.2 mg/L ampicillin (Sigma), *P. aeruginosa* PA01 was enumerated on Difco *Pseudomonas* selective agar (BD, Sparks, MD), while *S. oneidensis* abundance was calculated as the difference between total live bacteria and the sum of *E. coli*, *P. aeruginosa* and *B. subtilis*.

Phage isolation, screening and characterization. SM buffer was used for phage harvest, storage and dilution. [23] The double-layer plaque (DLP) assay was adopted for phage enumeration as plaque-forming-units (PFU). Polyvalent phages infecting both *E. coli* and *P. aeruginosa* were isolated from wastewater using a sequential multiple-host approach. [23] The phage library went through the sequence of *E. coli* > *P. aeruginosa* > *E. coli* + *P. aeruginosa* (Fig. 1A). The clear plaques on the multi-species bacterial lawn were harvested in SM buffer and purified by filtration through MILLEX 0.22-μm membrane (Millipore, Tullagreen, IRL).

Purified phages were subject to biofilm diffusion assays to screen phages with high biofilm propagation potential. [24] Briefly, phage suspensions (10^6 PFU/well) were poured on the top of dual species biofilm of *E. coli* and *P. aeruginosa* and then further incubated for 6 h to allow the phages to spread across the biofilm (Fig. S1A). The solution in the bottom chamber was collected every hour and the phage concentration was counted by the DLP assay. Two phage candidates (PEB1 and PEB2) reaching the bottom chamber within 6 h (Fig. S1B) were characterized in terms of morphology, efficiency of plating (EOP), and major growth parameters (i.e., adsorption rate, latent time and burst size) as previous reported. [23]

Magnetic CNCs syntheses, modification, and characterization. Magnetic CNCs of three

different sizes (150, 250, and 500 nm, as shown in Fig. 2) were synthesized using solvothermal reactions by varying the diethylene glycol (DEG) to ethylene glycol (EG) volume to volume ratio in their respective syntheses. [29, 30] The CNCs were functionalized with (3-aminopropyl) triethoxysilane (APTES) by a sol-gel reaction according to a previously reported procedure. [31] The morphology and size distribution were observed with a JEOL 2010 transmission electron microscope (TEM) at 200 kV and size distributions of CNCs were estimated based on 100 particles under TEM. The crystalline compositions were identified by powder X-ray diffraction (XRD, Rigaku DMAX) with Cu Kα radiation (λ = 1.54178 A). Characterization of the amino groups at the surface of the CNCs was done by Fourier transform infrared (FTIR) spectra using FTIR Microscope (Nicolet iS50 FTIR, Thermo Scientific). The zeta potentials were measured by a Nanosized Zetasizer instrument (Malvern Instruments). Surface elements were analyzed by X-ray photoelectron spectroscopy (XPS) using a PHI Quantera SXM scanning X-ray microprobe system. Magnetic characterization was conducted with a Superconducting Quantum Interference Device (SQUID) completed with a Magnetic Property Measurement System (MPMS XL, Quantum Design Inc.). For each measurement, the samples were weighed, wrapped in Teflon tape, and measured from -10 kOe to 10 kOe at 300 K. The size and surface parameters of CNCs are summarized in Table 1.

PNCs construction and characterization. PNCs were constructed by covalent binding between the phages and CNCs (amide bonds) activated by N-hydroxysuccinimide (NHS) and 1-ethyl-3-(3-(dimethylamino)propyl)carbodiimide hydrochloride (EDC) [14, 15] Specifically, CNCs (1 mL, 1 mg/mL PBS buffer), EDC (200 μL, 20 mg/mL), NHS (100 μL, 20 mg/mL) and phage

(1 mL, 10^9 PFU/mL PBS buffer) were mixed and rotated at 30 rpm for 12 h at 4 °C. After the reaction, the PNCs were collected by magnets (K&J Magnetics, 600 gauss) and the loosely bound phages were washed out twice with 4 °C PBS. Conjugation was confirmed by epifluorescence microscopy (EFM) using SYBR Gold-stained phage particles (Fig. 3). The PNCs were resuspended with PBS and loaded on Al_2O_3 Anodisc membrane filter (Whatman, Clifton, NJ). The sample was mounted on a glass slide with a drop of ProLong Gold Antifade reagent (Invitrogen) and observed under an EFM (Olympus IX71).

Phages in the initial supernatant and washing solution were mixed to enumerate the total residual phages. The number of phages loaded onto CNCs was calculated as the difference between the added and the total residual phage amount. Each PNC regardless of number of phages loaded served as an infectious center[16, 17] and would form a single plaque on the bacterial lawn in DLP assay.[32] Therefore, the number of PNCs was measured by the DLP assay and each plaque was counted as one PNC. The phage loading capacity was determined as the maximum number of loaded phages divided by the number of infectious centers (i.e., PNCs number). The phage loading efficiency of each sized CNCs was defined as the number of phages attached per unit surface area.

Bacterial challenge tests in dual species biofilm conditions. A dual species biofilm (*E. coli* and *P. aeruginosa*, which are hosts to both phages) was established on microtiter plates (Grace Bio-Labs, Bend, OR). Bacteria in exponential phase (10 μL for each strain, OD_{600} = 0.1) were cultivated in 180 μL M63 glucose medium. Plates were incubated at 30 °C while shaking at 100 rpm. The liquid medium was replaced with fresh medium every 12 h. After 48-h cultivation,

unattached cells were gently washed away by PBS buffer, and the biofilms were treated with following agents: (1) Free phages (2×10^5 PFU per well), (2) large-sized PNCs, (3) medium-sized PNCs, and (4) small-sized PNCs. The PNCs were pushed into the biofilm by a 600-gauss magnetic field. Phage-free CNCs had no noticeable antifouling or bactericidal effects based on crystal violet biofilm assay and bacterial growth curves (Fig. S2).

After 6-h treatment, the remaining biomass was estimated by crystal violet optical assay as previously reported.[10] The biofilm removal efficiency (%) was calculated as the relative difference between the OD_{595} values of treated biofilm and control biofilm. Experiments were done in parallel to enumerate phage numbers. To disperse the matrix-entrapped phages, Tween-20 was added to a final concentration of 0.05% (v/v), and gently sonicated at 40 kHz for 5 min in a 4°C bath sonicator (Branson, Danbury, CT). The final phage counts in each well were measured by the DLP assay using *E. coli* and *P. aeruginosa* as hosts.

Numerical model construction, calibration and simulation. To simulate biofilm eradication by PNCs, one semi-empirical stochastic spatial model was established as follows. One two-dimension checkerboard was used to represent the cross-section of biofilm (100 grids in width and 12 grids in height). Each grid can be occupied by at most one bacterium, and the upper limit for phage number was set at 780 per grid (assuming the grid is filled with phage PEB1). PNCs were dispersed as Fig. S3 following normal distribution at the bottom of biofilm.[20] The bacteria-phage interactions simulated by our modified model consider the following phenomena: (I) Bacterial infection by phage and phage number increased by burst size (Eqn. 1), (II) phage diffusion in horizontal and vertical directions (Eqn. 2), and (III) phage trap by biofilm matrix

(Eqn. 3). All these phage processes were assumed to follow Poisson processes (P_α, P_λ and P_δ are the probabilities of phage infection, phage diffusion and phage degradation, respectively).[18, 20] Diffusion rate and degradation/trap rate are different in the horizontal and vertical directions because vertical channels may be generated (which facilitate phage diffusion and mitigate phage trap) when PNCs penetrate the biofilm [33-35]

$$P_\alpha = 1 - \exp\left(-\alpha N_0\left(\frac{1-\exp\left(-\delta\Delta t\right)}{\delta}\right)\right) \quad (1)$$

$$P_\lambda = 1 - \frac{e^{-\lambda_H \Delta t} + e^{-\lambda_V \Delta t}}{2} \quad (2)$$

$$P_\delta = 1 - \frac{e^{-\delta_H \Delta t} + e^{-\delta_V \Delta t}}{2} \quad (3)$$

$$\lambda_V = \lambda_H \times (1 + F_\lambda) \quad (4)$$

$$\delta_V = \delta_H \times (1 - F_\delta) \quad (5)$$

Where N_0 is initial phage number, α is infection rate coefficient, δ is degradation/trap rate coefficient, λ_H is horizontal diffusion rate coefficient, λ_V is vertical diffusion rate coefficient, δ_H is horizontal trapping rate coefficient, δ_V is vertical trapping rate coefficient, F_λ is facilitation coefficient for phage diffusion, F_δ is facilitation coefficient for phage trapping, and Δt is the size of each time step. The parameters in this model (Table 2) were obtained either from experimental measurement or from previous studies[18, 36] rather than data fitting. The model was calibrated by experimental results of biofilm removal and phage replication. The major effects of physical disruption by PNCs (Figs. S4 and S5) were reflected by increased phage diffusion (Eqn. 4) and decreased phage trapping (Eqn. 5) in the vertical direction that the magnetic field was applied. Detailed information about this model is provided in the supporting information.

Nonetheless, limitations of semi-empirical models resulting from simplifying assumptions

should be recognized. This model assumes homogeneous biofilms and does not consider physical and ecological heterogeneities (including those caused by penetration by PNCs of different sizes) or spatial and temporal variations of model parameters. Whereas such limitations hinder accurate system-specific prediction capabilities, this model is useful to interpret experimental results and provide valuable insight on biofilm penetration and phage propagation dynamics.

Multiple-species biofilm growth and removal tests. One standard CDC biofilm reactor with polypropylene coupons was used to grow multiple species biofilm at 25 °C with magnetically stirring at 60 rpm. The reactor was filled with M63 medium inoculated with *E. coli*, *P. aeruginosa*, *B. subtilis*, and *S. oneidensis* (10 μL for each strain with initial OD_{600} = 0.1) and allowed bacteria to colonize onto the coupons for 24 h. After that, fresh M63 medium was continuously pumped into the reactor at 2 mL/min with a Masterflex peristaltic pump (Cole-Parmer, IL) for 72 h. The 4-day multi-species biofilm on coupons was washed gently with PBS and then subject to phage tests in Corning 24-well plates (Sigma, MO). The biofilms were treated for 6 h as follows: (1) Free phage PEB1 (10^6 PFU per well), (2) large PNCs with 10^6 PFU PEB1 immobilized, (3) small PNCs with same surface area for phage immobilization. After treatment, three coupons were used for biofilm mass measurement using the crystal violet optical assay, and the other three coupons were used for bacterial enumeration. The biofilm was dispersed by sonication at 4°C in PBS buffer with 0.5% Tween 20, and the detached bacteria were enumerated using viable plate counts of total and individual species (EMB agar for *E. coli* and *Pseudomonas* agar for *P. aeruginosa*).

To visualize the extent of biofilm removal, the residual biofilm on coupon was fixed then stained with SYTO 9 and propidium iodide (PI) from LIVE/DEAD BacLight kit (Invitrogen, Basel, Switzerland) following the manufacturer's instructions. The stained biofilm was placed on a slide, immersed in ProLong Gold antifade mounting media (Thermo Fischer Scientific) and covered with a confocal approved coverslip No. 1.5 (VWR, USA). The sample was loaded on a customized sample holder and then observed using 40X dry objective under Nikon A1-Rsi confocal laser scanning microscopy- CLSM (Nikon, Tokyo, Japan). The biofilm was excited using 488 nm laser line then visualized in green channel (500-550 nm) for live bacteria and using 560 nm laser line excitation then visualized in red channel (570-620 nm) for dead bacteria. The biofilm bottom layers were scanned to investigate the impacts of different sized PNCs on biofilm disruption. Z-stack images were collected and rendered into three-dimension (3D) images to visualize the structure of biofilm using Nikon NIS-Element software (Nikon, Tokyo, Japan).

RESULTS AND DISCUSSION

Biofilm diffusion assay selected for phages with desirable traits for biofilm treatment. The presence of multiple bacterial species (many of which are nor recognized or infected by specific phages) and their EPS (which represents a diffusion barrier) contribute to biofilm resistance to phages.[10, 37] Moreover, bacteria in the inner layers of biofilms exhibit lower metabolic activities,[38] hindering phage propagation. Thus, phages with broad host range, depolymerase enzymatic activity to degrade EPS, and low dependence on host metabolism are preferred for biofilm eradication.[39]

Podoviridae phages PEB1 and PEB2 were obtained using the sequential multiple-host approach followed by biofilm diffusion assays (Fig. 1A). In biofilm phage diffusion assay, phage PEB1 and PEB2 propagated efficiently through the dual species biofilm of *E. coli* and *P. aeruginosa* and reached the collection chambers within 6 h (Fig. S1). Although PEB1 (54 nm in head diameter) was smaller than PEB2 (86 nm in head diameter) (Fig.1 B&C), both phages shared some beneficial features for infecting both *E. coli* and *P. aeruginosa* in biofilms. First, these phages exhibited high efficiency of infection towards both *E. coli* and *P. aeruginosa*: PEB1 had an EOP of 1.0 for *E. coli* and 0.76 for *P. aeruginosa*, while PEB2 had corresponding EOPs of 1.0 and 0.84. Phage plaques on the dual bacterial lawn were both clear in the center and surrounded with a halo (Fig.1 B&C), a strong indication of their ability to produce depolymerase against biofilm EPS.[40] Additionally, both phages could replicate in these hosts in stationary growth phase (Fig.1 B&C), which may facilitate phage infecting bacteria with reduced metabolic activities in mature biofilms.[41] Therefore, phages PEB1 and PEB2 were chosen from the candidates ($n > 10$) for PNCs construction and biofilm eradication studies.

Larger CNCs loaded more phages per particle, while smaller CNCs exhibited higher phage conjugation efficiency (phages per unit area).

CNCs surface amination provides covalent binding sites for the carboxylic groups on the phage head (i.e., amide bonds), exposing the phage tail for host infection.[13, 14] The FTIR spectra (Fig. 2C) shows absorption bands at 996 cm^{-1}, 1126 cm^{-1} , 1662 cm^{-1} and 3401 cm^{-1} corresponding to Si-O, SiO-H and N-H vibrations, respectively. [42] These data correspond to the APTES functionalized surface of the CNCs. [43] According to Scherrer's equation, X-ray diffraction

patterns show that the magnetite samples of 150, 250 and 500 nm are formed by crystallites of 15 nm, 34 nm, and 13 nm, respectively (Fig. 2B).[44] Additionally, these CNCs showed magnetization saturation values in the range of 60 to 100 emu/g at room temperature corresponding to superparamagnetic-like behavior (Fig. 2D).[45] This observed magnetic behavior can help phages penetrate through biofilms under relatively low-strength magnetic fields.

Three different sized magnetic CNCs were tested for phage loading capacity and phage conjugation efficiency (Figs. 3B&C). EFM images show that non-fluorescent CNCs emit green fluorescence after conjugation with SYBR-stained PEB1 (Fig. 3A). The number of phages loaded onto each sized CNCs was proportional to the size of the CNCs (Fig. 3B), which is reflected by the intensity of green fluorescence from the PNCs with DNA-stained phages. For phage PEB1, about 4±1, 12±2 and 37±2 phages were loaded per 150, 250 and 500 nm CNCs, respectively. For phage PEB2 with similar surface charge but larger size (Table 1), about 2±1, 7±2 and 26±3 phages were loaded per 150, 250 and 500 nm CNCs, respectively (Fig. 3B). Each CNC loaded more PEB1 than PEB2 phages, possibly due to less steric hindrance and electrostatic repulsion between the smaller phage particles on CNC surfaces.[14]

Although the larger CNCs (with higher surface area per particle) exhibit significantly higher phage loading capacity, higher efficiency of phage immobilization (phages attached per unit area) was observed in the smaller CNCs (150 and 250 nm) for phage PEB1 (Fig. 3C). Specifically, the phage loading efficiency of 150, 250 and 500 nm CNCs was about 60±4, 62±5, and 47±4 phage particles/μm^2, respectively. The higher loading efficiency of the smaller CNCs may be attributed to the higher specific surface area and more amino group (active sites for

phage covalent binding) (Table 1). The loading efficiency for the larger PEB2 was similar across the different CNCs sizes (41±3, 44±4, and 37±3 phage particles/μm^2 for 150, 250 and 500 nm CNCs, respectively). The higher amino group density on smaller CNCs did not result in higher phage loading efficiency for PEB2. Specifically, PEB2 with a relatively large size might have an increased electrostatic repulsion and steric hindrance on the smaller CNCs, which would offset the advantage of more amino group on the smaller CNCs. Increased repulsion among these negatively charged phages surfaces presumably leads to relatively even phage distribution.[46]

Small PNCs facilitated phage propagation and enhanced dual species biofilm removal. Phages act as self-replicating antibacterial agents in the presence of proper bacterial hosts. After treatment with free phages for 6 h, the biofilm mass was reduced by 37.7±3.2 % with PEB1and 35.4±2.4 % with PEB2 (Fig. 4A). PEB1 and PEB2 titters increased from 1.0×10^6 to $4.0\pm0.3 \times 10^8$ and $3.8\pm0.3 \times 10^8$ PFU/mL, respectively (Fig. 4B). During free phage treatment, the liquid solution likely diluted the phage density at the interface of biofilm and bulk solution, [15] and bacterial debris and EPS matrix could hinder phage diffusion deep into the biofilm.[47] These limitations were overcome by loading properly oriented phages onto magnetic nanocomposites and pushing them with a magnetic field to the inner layer of the biofilm. When a similar number of PEB1 phages were loaded onto the large CNCs and penetrated the biofilm under a magnetic field, phage propagation was facilitated and final phage counts increased to $6.8\pm0.4 \times 10^8$ PFU/mL, with a higher biofilm removal efficiency of 80.2±3.4 ±1.4 %.

Though each large PNC loaded more phages per particle, there was no benefit to loading additional phages after the threshold for initiating infection was reached (e.g., same biofilm

removal efficiency for 22 and 38 phages per particle, Fig. S6). Small PNC with 4 PEB1 conjugated per particle on average facilitated phage propagation in the tested biofilm due to higher dispersion, resulting in final phage counts of 8.8±0.4× 10^8 PFU/mL and biofilm removal efficiency 96.3±1.4 %. On the other hand, large PNCs physically disrupted the biofilm to a greater extent than small PNCs (Fig. S4), which facilitated phage diffusion in the vertical direction (Fig. S1B), although this advantage was offset by lower horizontal diffusion (Fig. 5C). Overall, phage propagation and biofilm removal were enhanced compared to free phage treatment, and small PNCs with higher horizontal dispersion in the deeper biofilm layers and sufficient phage loading to initiate infection were better suited for treating biofilms.

Small PNCs loaded with fewer large phages were less effective than those loaded with a larger number of smaller phages. Specifically, comparing small PNCs loaded on average with 4 (smaller) PEB1 or 2 (larger) PEB2 per particle, the PEB1-loaded PNCs reached higher biofilm removal efficiency (96.3±1.4 % vs. 85.4±3.2 %) and larger final phage titter (8.8±0.4 × 10^8 vs. 6.9±0.4 ×10^8 PFU/mL) than PNCs loaded with PEB2 phages. However, this trend was not observed for large PNCs loaded with 38 PEB1 versus 26 PEB2 per particle. In both cases, large PNCs carried sufficient phages to initiate infection, and there were no noticeable drawbacks to replacing smaller phages with fewer larger phages (Fig. 4).

The semi-empirical model infers distinct phage infection patterns by different sized PNCs. Our model infers that free phages and PNCs followed different propagation patterns to disrupt the biofilm (Fig.S7). The simulated results agree with the residual biofilm patterns observed experimentally (Fig. 5). In these simulations, free phages proliferated towards biofilm inner

layers but did not efficiently reach the bottom within the treatment period, which resulted in significant residual biofilm (Fig. S7A). In contrast, PNCs initiate infection at the bottom and proliferate upwards, leading to disruption of the inner layers and de-anchoring of the biofilm, resulting in more efficient biofilm eradication (Figs. S7B-D).

Based on the semi-empirical model, different sized PNCs caused distinct phage infection patterns because of differences in numbers of infection centers and extent of vertical biofilm penetration. Large PNCs resulted in greater vertical phage penetration and significant biofilm clearance where PNCs were introduced (Fig. 5C). However, due to relatively low horizontal propagation, there were some inner layer areas not reached by phages (Fig. 5C). Fluorescent imaging agreed with simulation results in that some residual biofilm areas contained live bacteria after treatment with large PNCs (Fig. 5C). In contrast, smaller PNCs distributed phages more evenly, forming more initial infection centers and exhibiting higher horizontal dispersion that cleared the biofilm bottom (Figs. 5D&E). The resulting more significant disruption of biofilm inner layers eradicated the biofilm within 6 h (Figs. 5D&E). Fluorescent imaging also showed less residual biofilm after treatment with smaller-sized PNCs (Figs. 5D&E).

PNCs eradicated a multi-species biofilm by targeting dominant species at the bottom layer. Maturation of biofilm and presence of phage-resistant bacteria hinders eradication by free phages.[48, 49] For example, mature multi-species biofilm containing soil bacteria exhibited improved resistance to phage infection relative to a dual species biofilm.[10] Treatment with free phage PEB1 for 6 h resulted in only 20.8±3.8 % removal efficiency for the multi-species biofilm, compared to 37.7±3.2 % for the above dual species biofilm.

PNCs pushed in by a 600-gauss magnetic field circumvented the defense of upper layer biofilm components and directly targeted the dominant bacteria that anchored the biofilm. After 3-h phage infection, the biofilm inner layer was disrupted to a much higher extent by PNCs than by free phages (Fig. 6A). Similar as with the dual species biofilm, small PNCs formed more infectious centers since they were more evenly distributed through this biofilm than large PNCs (Fig. 6A).

Following a bottom-up phage propagation pattern, PNCs may destabilize and de-anchor the whole biofilm following lysis of the inner layer bacteria and degradation of the EPS matrix. After 6-h treatment, biofilm removal was 67.6±3.8 % with large PNCs and 94±3.1 % with small PNCs (Fig. 6B). Although large PNCs significantly improved biofilm removal efficiency compared to free phages, the presence bacteria resistant to these phages (*B. subtilis* and *S. oneidensis*) and accumulation of dead bacteria (Figs. 6B&C) hindered phage propagation[18]. Due to higher horizontal phage distribution, small PNCs resulted in more thorough biofilm removal with a significantly lower abundance of live bacteria (green cells under CLSM) in the residual biofilm (Fig. 6 B&C). Additionally, the dominance of *E. coli* and *P. aeruginosa* was replaced by that of phage-resistant *B. subtilis* and *S. oneidensis* after PNC treatment (Fig. 6B).

CONCLUSIONS

Current biofilm removal approaches are relatively inefficient, which calls for more effective and sustainable biofilm-eradication technologies. Coupling multi-host isolation methods with biofilm phage diffusion assays selected for phages with broad host range and high biofilm propagation potential to facilitate biofilm eradication. Magnetic phage-nanocomposite conjugates (PNCs) driven by a magnetic field initiate phage infection at the biofilm bottom, leading to rapid biofilm detachment. A semi-empirical numerical model appropriately simulated the phage propagation patterns, and corroborated the observed biofilm removal efficiency by different sized PNCs: small PNCs effectively de-anchored the biofilm through extensive horizontal dispersion through the bottom of the biofilm, while large PNCs exerted larger biofilm disruption in the vertical direction. This combined computational and experimental approach demonstrates an inverse relationship between PNC size and biofilm eradication potential, and provides mechanistic insight for the application of nanotechnology-enhanced phage-based biofilm control.

ACKNOWLEDGMENTS

This study was supported by the NSF ERC on Nanotechnology-Enabled Water Treatment (EEC-1449500), and by NSF PIRE grant (OISE-1545756). We thank Laurel Bingman, Bo Zhang and Xifan Wang for their help with phage and material characterization, and Alloysius J. Budi Utama and Ling-li Li for helping with biofilm imaging and analyses.

REFERENCES

1. K. Kimura, N. Yamato, H. Yamamura and Y. Watanabe, Membrane Fouling in Pilot-Scale Membrane Bioreactors (MBRs) Treating Municipal Wastewater, *Environ. Sci. Technol.*, 2005, **39**, 6293-6299.
2. S. Liu, C. Gunawan, N. Barraud, S. A. Rice, E. J. Harry and R. Amal, Understanding, Monitoring, and Controlling Biofilm Growth in Drinking Water Distribution Systems, *Environ. Sci. Technol.*, 2016, **50**, 8954-8976.
3. M. B. Waak, T. M. LaPara, C. Hallé and R. M. Hozalski, Occurrence of *Legionella spp.* in Water-Main Biofilms from Two Drinking Water Distribution Systems, *Environ. Sci. Technol.*, 2018, **52**, 7630-7639.
4. T. Schwartz, W. Kohnen, B. Jansen and U. Obst, Detection of Antibiotic-Resistant Bacteria and Their Resistance Genes in Wastewater, Surface Water, and Drinking Water biofilms, *FEMS Microbiol. Ecol.*, 2003, **43**, 325-335.
5. F. Yang, B. Shi, Y. Bai, H. Sun, D. A. Lytle and D. Wang, Effect of Sulfate on the Transformation of Corrosion Scale Composition and Bacterial Community in Cast Iron Water Distribution Pipes, *Water Res.*, 2014, **59**, 46-57.
6. Z. Xue, C. M. Hessler, W. Panmanee, D. J. Hassett and Y. Seo, *Pseudomonas aeruginosa* Inactivation Mechanism is Affected by Capsular Extracellular Polymeric Substances Reactivity with Chlorine and Monochloramine, *FEMS Microbiol. Ecol.*, 2013, **83**, 101-111.
7. G. McDonnell and A. D. Russell, Antiseptics and Disinfectants: Activity, Action, and Resistance, *Clin. Microbiol. Rev.*, 1999, **12**, 147-179.
8. J. Mathieu, P. Yu, P. Zuo, M. L. B. Da Silva and P. J. J. Alvarez, Going Viral: Emerging Opportunities for Phage-Based Bacterial Control in Water Treatment and Reuse, *Acc. Chem. Res.*, 2019, **52**, 849-857.
9. A. C. Gregory, A. A. Zayed, N. Conceição-Neto, B. Temperton, B. Bolduc, A. Alberti, M. Ardyna, K. Arkhipova, M. Carmichael, C. Cruaud, C. Dimier, G. Domínguez-Huerta, J. Ferland, S. Kandels, Y. Liu, C. Marec, S. Pesant, M. Picheral, S. Pisarev, J. Poulain, J.-É. Tremblay, D. Vik, S. G. Acinas, M. Babin, P. Bork, E. Boss, C. Bowler, G. Cochrane, C. de Vargas, M. Follows, G. Gorsky, N. Grimsley, L. Guidi, P. Hingamp, D. Iudicone, O. Jaillon, S. Kandels-Lewis, L. Karp-Boss, E. Karsenti, F. Not, H. Ogata, S. Pesant, N. Poulton, J. Raes, C. Sardet, S. Speich, L. Stemmann, M. B. Sullivan, S. Sunagawa, P. Wincker, M. Babin, C. Bowler, A. I. Culley, C. de Vargas, B. E. Dutilh, D. Iudicone, L. Karp-Boss, S. Roux, S. Sunagawa, P. Wincker and M. B. Sullivan, Marine DNA Viral Macro- and Microdiversity from Pole to Pole, *Cell*, 2019, **177**, 1109-1123.e1114.
10. P. Yu, J. Mathieu, Y. Yang and P. J. J. Alvarez, Suppression of Enteric Bacteria by Bacteriophages: Importance of Phage Polyvalence in the Presence of Soil Bacteria, *Environ. Sci. Technol.*, 2017, **51**, 5270-5278.
11. I. W. Sutherland, K. A. Hughes, L. C. Skillman and K. Tait, The Interaction of Phage and Biofilms, *FEMS Microbiol. Lett.*, 2004, **232**, 1-6.

12. P. A. de Jonge, F. L. Nobrega, S. J. Brouns and B. E. Dutilh, Molecular and Evolutionary Determinants of Bacteriophage Host Range, *Trends Microbiol.*, 2018.
13. Z. Hosseinidoust, A. L. J. Olsson and N. Tufenkji, Going Viral: Designing Bioactive Surfaces with Bacteriophage, *Colloids Surf. B. Biointerfaces*, 2014, **124**, 2-16.
14. S. Bone, A. Alum, J. Markovski, K. Hristovski, E. Bar-Zeev, Y. Kaufman, M. Abbaszadegan and F. Perreault, Physisorption and Chemisorption of T4 Bacteriophages on Amino Functionalized Silica Particles, *J. Colloid Interface Sci.*, 2018, **532**, 68-76.
15. L.-L. Li, P. Yu, X. Wang, S.-S. Yu, J. Mathieu, H.-Q. Yu and P. J. J. Alvarez, Enhanced Biofilm Penetration for Microbial Control by Polyvalent Phages Conjugated with Magnetic Colloidal Nanoparticle Clusters (CNCs), *Environ. Sci. Nano.*, 2017, **4**, 1817-1826.
16. B. P. Taylor, C. J. Penington and J. S. Weitz, Emergence of Increased Frequency and Severity of Multiple Infections by Viruses Due to Spatial Clustering of Hosts, *Phys. Biol.*, 2017, **13**, 066014.
17. N. Mitarai, S. Brown and K. Sneppen, Population Dynamics of Phage and Bacteria in Spatially Structured Habitats Using Phage λ and *Escherichia coli*, *J. Bacteriol.*, 2016, **198**, 1783.
18. S. Heilmann, K. Sneppen and S. Krishna, Coexistence of Phage and Bacteria on the Boundary of Self-Organized Refuges, *Proc. Natl. Acad. Sci. U.S.A.*, 2012, **109**, 12828.
19. R. S. Eriksen, N. Mitarai and K. Sneppen, Sustainability of Spatially Distributed Bacteria-Phage Systems, *bioRxiv*, 2019, 495671.
20. P. Roychoudhury, N. Shrestha, R. Wiss Valorie and M. Krone Stephen, Fitness Benefits of Low Infectivity in A Spatially Structured Population of Bacteriophages, *Proc. R. Soc. Lond. B. Biol. Sci.*, 2014, **281**, 20132563.
21. B. Ashby, S. Gupta and A. Buckling, Spatial Structure Mitigates Fitness Costs in Host-Parasite Coevolution, *Am. Nat.*, 2014, **183**, E64-E74.
22. M. Simmons, K. Drescher, C. D. Nadell and V. Bucci, Phage Mobility is A Core Determinant of Phage-Bacteria Coexistence in Biofilms, *ISME. J.*, 2018, **12**, 531-543.
23. P. Yu, J. Mathieu, M. Li, Z. Dai and P. J. J. Alvarez, Isolation of Polyvalent Bacteriophages by Sequential Multiple-Host Approaches, *Appl. Environ. Microbiol.*, 2016, **82**, 808.
24. S. González, L. Fernández, D. Gutiérrez, A. B. Campelo, A. Rodríguez and P. García, Analysis of Different Parameters Affecting Diffusion, Propagation and Survival of Staphylophages in Bacterial Biofilms, *Front. Microbiol.*, 2018, **9**.
25. K. K. Kumarasamy, M. A. Toleman, T. R. Walsh, J. Bagaria, F. Butt, R. Balakrishnan, U. Chaudhary, M. Doumith, C. G. Giske, S. Irfan, P. Krishnan, A. V. Kumar, S. Maharjan, S. Mushtaq, T. Noorie, D. L. Paterson, A. Pearson, C. Perry, R. Pike, B. Rao, U. Ray, J. B. Sarma, M. Sharma, E. Sheridan, M. A. Thirunarayan, J. Turton, S. Upadhyay, M. Warner, W. Welfare, D. M. Livermore and N. Woodford, Emergence of A New Antibiotic Resistance Mechanism in India, Pakistan, and the UK: A Molecular, Biological, and Epidemiological Study, *Lancet. Infect. Dis.*, 2010, **10**, 597-602.

26. T.-F. Mah, B. Pitts, B. Pellock, G. C. Walker, P. S. Stewart and G. A. O'Toole, A Genetic Basis for *Pseudomonas aeruginosa* Biofilm Antibiotic Resistance, *Nature*, 2003, **426**, 306-310.
27. A. M. Earl, R. Losick and R. Kolter, Ecology and Genomics of *Bacillus subtilis*, *Trends Microbiol.*, 2008, **16**, 269-275.
28. J. L. Groh, Q. Luo, J. D. Ballard and L. R. Krumholz, Genes That Enhance the Ecological Fitness of *Shewanella oneidensis* MR-1 in Sediments Reveal the Value of Antibiotic Resistance, *Appl. Environ. Microbiol.*, 2007, **73**, 492-498.
29. L. Zhuang, W. Zhang, Y. Zhao, H. Shen, H. Lin and J. Liang, Preparation and Characterization of Fe_3O_4 Particles with Novel Nanosheets Morphology and Magnetochromatic Property by a Modified Solvothermal Method, *Sci. Rep.*, 2015, **5**, 9320.
30. P. Hu, L. Yu, A. Zuo, C. Guo and F. Yuan, Fabrication of Monodisperse Magnetite Hollow Spheres, *J. Phys. Chem. C.*, 2009, **113**, 900-906.
31. H. Yang, L. Qin, Y. Wang, B. Zhang, Z. Liu, H. Ma, J. Lu, X. Huang, D. Shi and Z. Hu, Detection of *Mycobacterium tuberculosis* Based on H(37)R(v) Binding Peptides Using Surface Functionalized Magnetic Microspheres Coupled with Quantum Dots – A Nano Detection Method for Mycobacterium Tuberculosis, *Int J Nanomedicine*, 2015, **10**, 77-88.
32. R. S. Eriksen, S. L. Svenningsen, K. Sneppen and N. Mitarai, A Growing Microcolony Can Survive and Support Persistent Propagation of Virulent Phages, *Proc. Natl. Acad. Sci. U.S.A.*, 2018, **115**, 337.
33. M. Simmons, K. Drescher, C. D. Nadell and V. Bucci, Phage Mobility is A Core Determinant of Phage–Bacteria Coexistence in Biofilms, *ISME. J.*, 2017, **12**, 531.
34. L. C. Coberly, W. Wei, K. Y. Sampson, J. Millstein, H. A. Wichman and S. M. Krone, Space, Time, and Host Evolution Facilitate Coexistence of Competing Bacteriophages: Theory and Experiment, *Am. Nat.*, 2009, **173**, E121-E138.
35. B. Kerr, C. Neuhauser, B. J. M. Bohannan and A. M. Dean, Local Migration Promotes Competitive Restraint in A Host–Pathogen 'Tragedy of The Commons', *Nature*, 2006, **442**, 75-78.
36. T.-O. Peulen and K. J. Wilkinson, Diffusion of Nanoparticles in a Biofilm, *Environ. Sci. Technol.*, 2011, **45**, 3367-3373.
37. T. K. Lu and J. J. Collins, Dispersing Biofilms with Engineered Enzymatic Bacteriophage, *Proc. Natl. Acad. Sci. U.S.A.*, 2007, **104**, 11197-11202.
38. P. S. Stewart and M. J. Franklin, Physiological Heterogeneity in Biofilms, *Nat. Rev. Microbiol.*, 2008, **6**, 199.
39. A. M. Motlagh, A. S. Bhattacharjee and R. Goel, Biofilm Control with Natural and Genetically-Modified Phages, *World J. Microbiol. Biotechnol.*, 2016, **32**, 67.
40. D. P. Pires, H. Oliveira, L. D. R. Melo, S. Sillankorva and J. Azeredo, Bacteriophage-Encoded Depolymerases: Their Diversity and Biotechnological Applications, *Appl. Microbiol. Biotechnol.*, 2016, **100**, 2141-2151.

41. D. Davies, Understanding Biofilm Resistance to Antibacterial Agents, *Nat. Rev. Drug. Discov.*, 2003, **2**, 114.
42. M. Shen, W. Jia, C. Lin, G. Fan, Y. Jin, X. Chen and G. Chen, Facile Synthesis of Folate-Conjugated Magnetic/Fluorescent Bifunctional Microspheres, *Nanoscale Res. Lett.*, 2014, **9**, 558.
43. E. Dezfoolinezhad, K. Ghodrati and R. Badri, Fe_3O_4@SiO_2@Polyionene/Br_3^- Core-Shell-Shell Magnetic Nanoparticles: A Novel Catalyst for the Synthesis of Imidazole Derivatives under Solvent-Free Conditions, *New J. Chem.*, 2016, **40**, 4575-4587.
44. C. S. Xavier, C. A. Paskocimas, F. V. d. Motta, V. D. Araújo, M. J. Aragón, J. L. Tirado, P. Lavela, E. Longo and M. R. B. Delmonte, Microwave-Assisted Hydrothermal Synthesis of Magnetite Nanoparticles with Potential Use as Anode in Lithium Ion batteries, *Mater. Res.*, 2014, **17**, 1065-1070.
45. L. Bogani, L. Cavigli, C. de Julián Fernández, P. Mazzoldi, G. Mattei, M. Gurioli, M. Dressel and D. Gatteschi, Photocoercivity of Nano-Stabilized Au:Fe Superparamagnetic Nanoparticles, *Adv. Mater.*, 2010, **22**, 4054-4058.
46. M. Dishon, O. Zohar and U. Sivan, From Repulsion to Attraction and Back to Repulsion: The Effect of NaCl, KCl, and CsCl on the Force between Silica Surfaces in Aqueous Solution, *Langmuir*, 2009, **25**, 2831-2836.
47. M. F. Hansen, S. L. Svenningsen, H. L. Røder, M. Middelboe and M. Burmølle, Big Impact of the Tiny: Bacteriophage–Bacteria Interactions in Biofilms, *Trends Microbiol.*, 2019, DOI: https://doi.org/10.1016/j.tim.2019.04.006.
48. S. Sillankorva, P. Neubauer and J. Azeredo, *Pseudomonas fluorescens* Biofilms Subjected to Phage PhiIBB-PF7A, *BMC Biotechnol.*, 2008, **8**, 79.
49. B. R. Levin and J. J. Bull, Population and Evolutionary Dynamics of Phage Therapy, *Nat. Rev. Microbiol.*, 2004, **2**, 166-173.

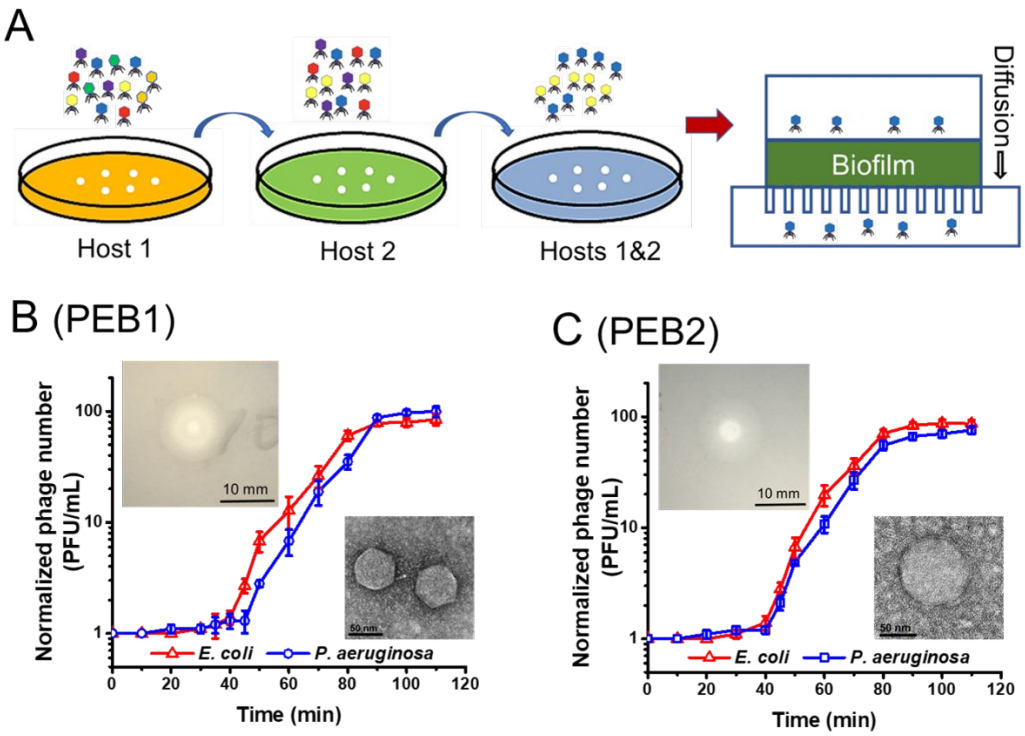

Figure 1. Isolation and screening of phages with high biofilm disruption capability. (A) Schematic illustration of sequential multiple-host phage isolation approach followed by phage biofilm diffusion assay. (B) The plaque of isolated phage PEB1 on DLP and its morphology under TEM. (C) The plaque of isolated phage PEB2 on DLP and its morphology under TEM. (B&C) One-step growth curves of phages PEB1 and PEB2 in bacterial hosts of stationary phase. Phage titers were normalized to the initial phage concentrations. Scale bar represents 50 nm in the TEM images.

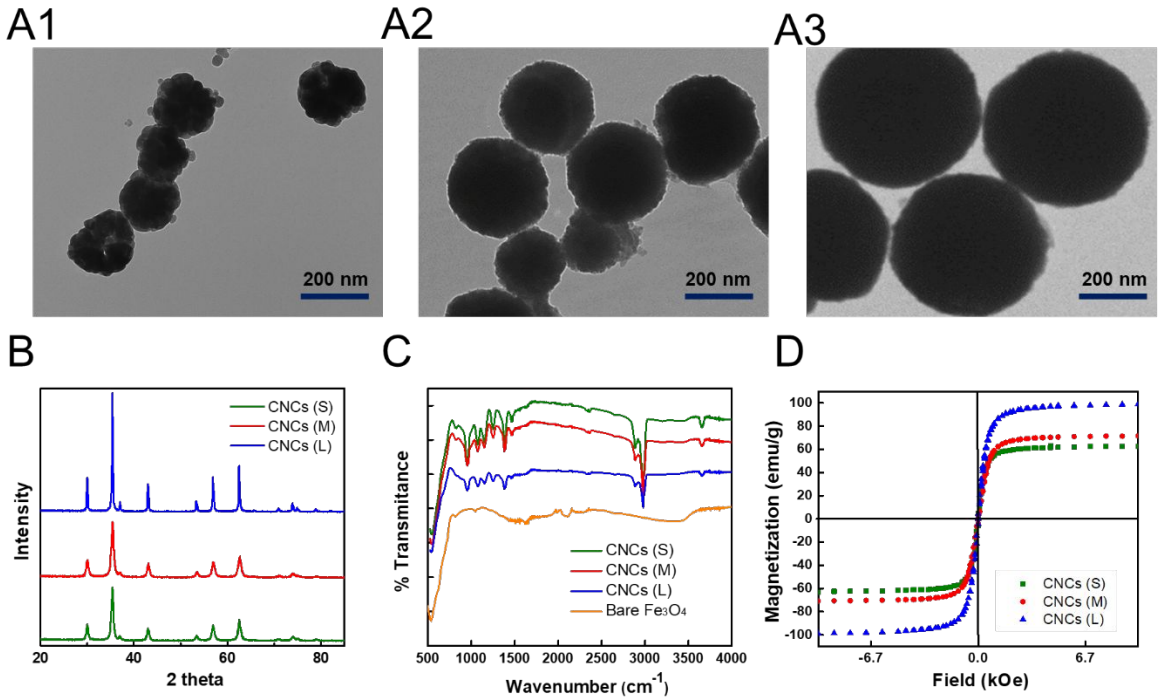

Figure 2. Characterization of Fe_3O_4@APTES magnetic colloidal nanoparticle clusters (CNCs). (A) SEM images of small Fe_3O_4@APTES CNCs (A1, 150 nm), medium Fe_3O_4@APTES CNCs (A2, 250 nm), and large Fe_3O_4@APTES CNCs (A3, 500 nm). The scale bars represent 200 nm. (B) XDR spectra, (C) FT-IR spectra, and (D) Magnetization curves of Fe_3O_4@APTES CNCs.

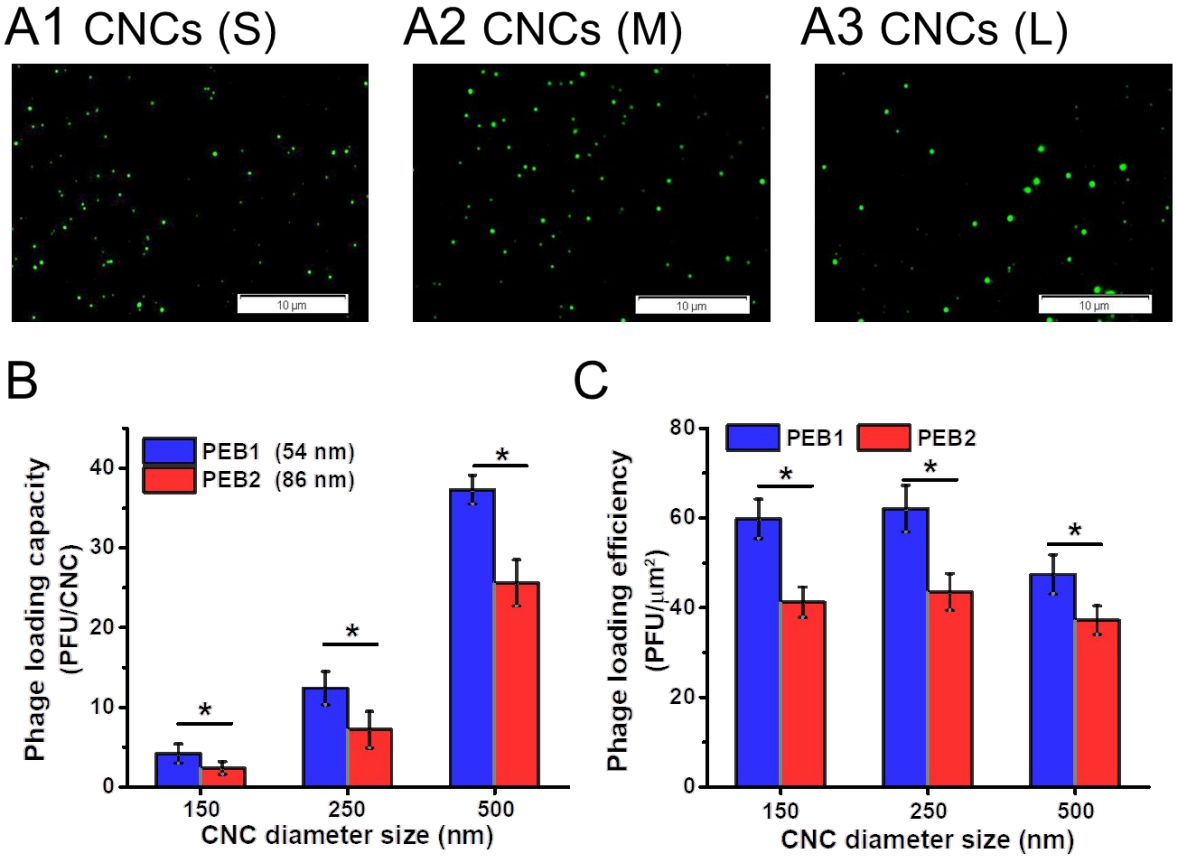

Figure 3. Confirmation and quantification of surface-bound phages onto CNCs. (A) Fluorescent images of SYBR Gold-stained phage PEB1 bound onto CNCs. The intensity of fluorescence was proportional to the size of the CNCs. The scale bar is 10 μm. (B) Phage loading capacity of CNCs with each larger CNC loading more phages, and (C) Phage loading efficiency (numbers of phages loaded per surface area) of different sized CNCs. Enumeration assays were performed three times, and the error bars denote mean ± one standard deviation.

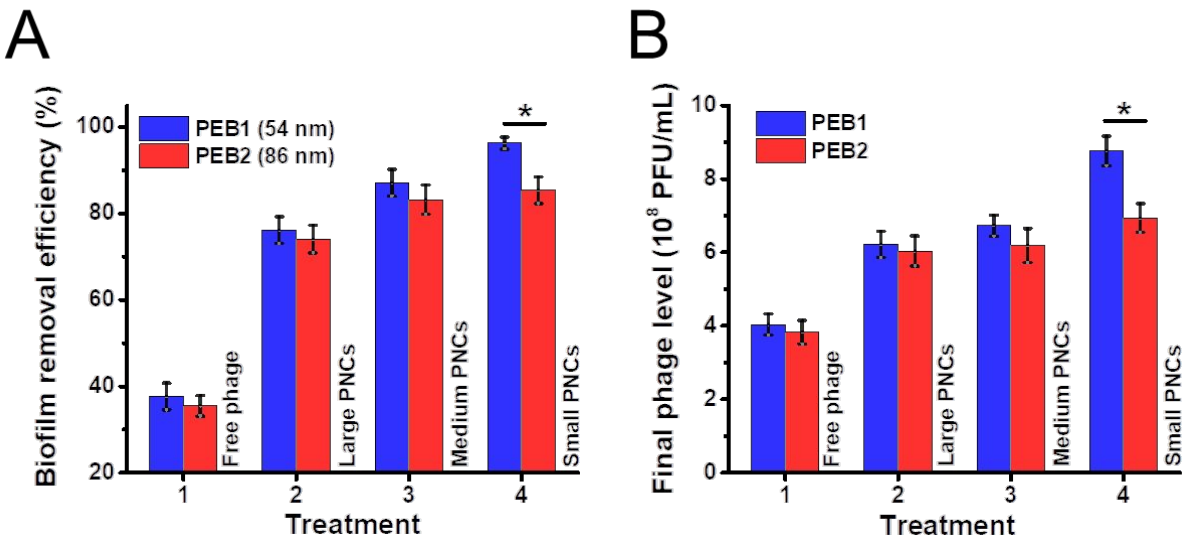

Figure 4. Biofilm removal and phage propagation after treatments with conjugated phages. The dual species biofilm of *E. coli* and *P. aeruginosa* was treated by different methods (1 – Free phages, 2 – Large PNCs, 3 –Medium PNCs, and 4 – Small PNCs). The CNCs have the same surface area for phage loading. Enumeration assays of biofilm mass and total phage counts were performed three times, and the error bars denote mean ± one standard deviation.

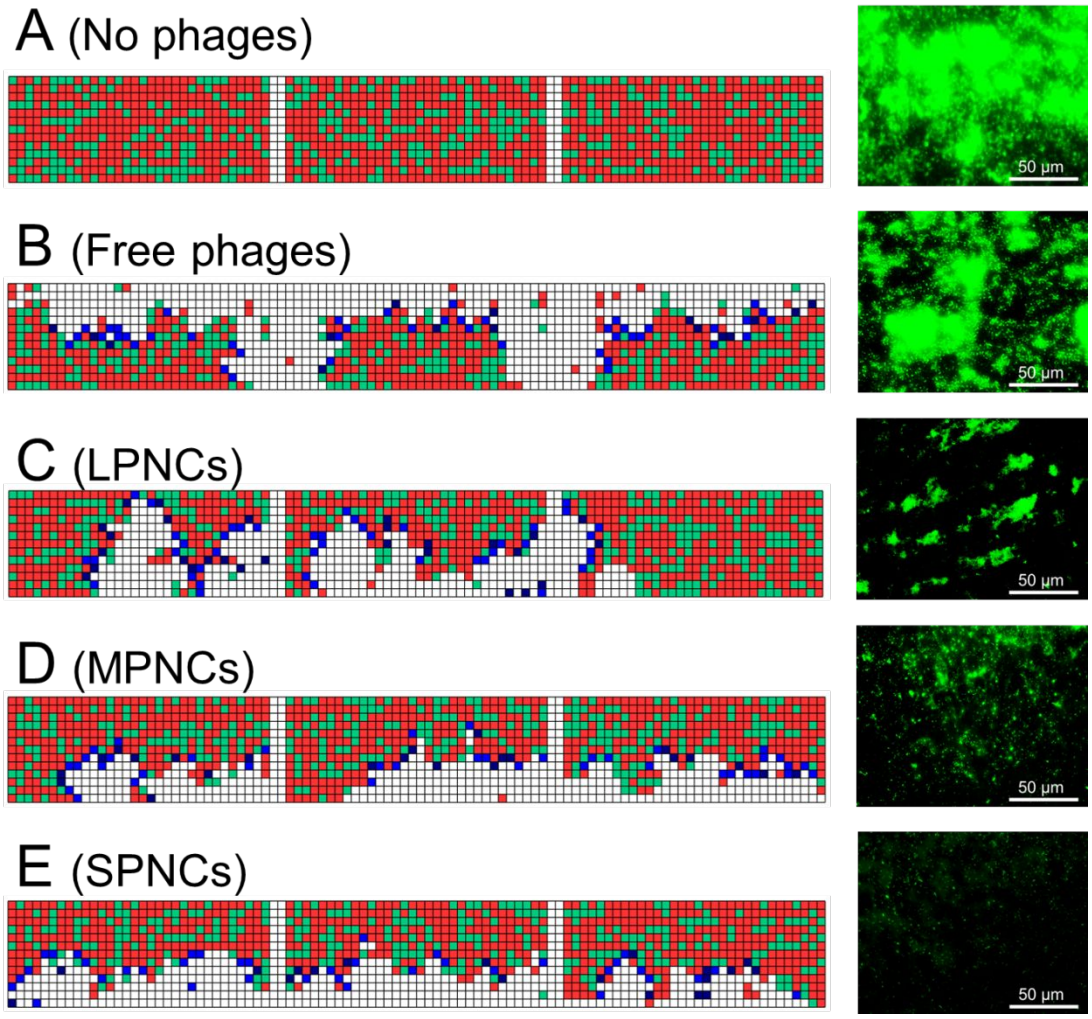

Figure 5. Simulation and experimental results of biofilm removal following treatment by free phages and different sized PNCs. The left panels are simulated cross-section of dual species biofilm of *E. coli* (red cell) and *P. aeruginosa* (green cell). The blue cells represent phage-infected bacteria that have not lysed yet. Each grid represents 0.5 × 0.5 μm. The right panels are microscopic images of the surface of residual biofilms stained with SYTO 9.

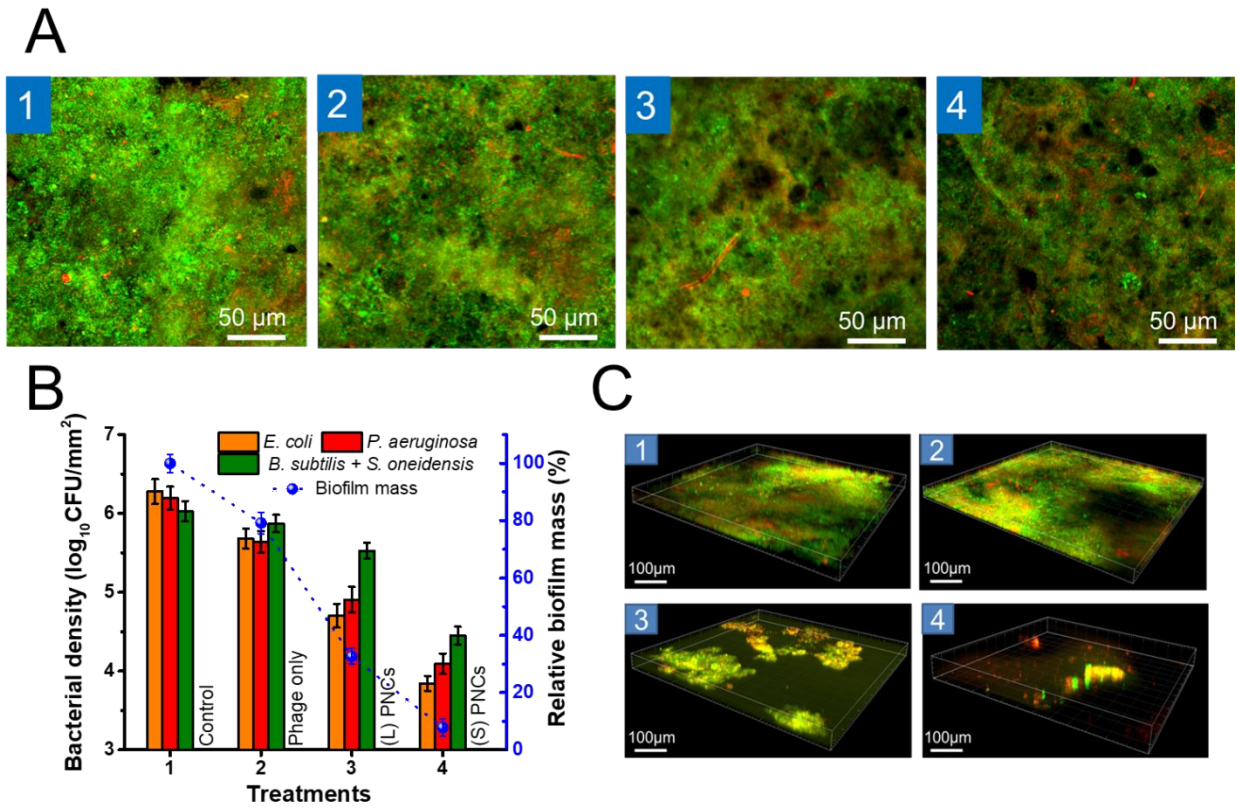

Figure 6. Mature biofilm disruption and eradication by free phages and PNCs. Four treatments are depicted: 1 – No phage added (control), 2 – Free phages, 3 – Large PNCs, 4 –Small PNCs. (A) Inner layer biofilm disruption by free phages and PNCs after 3-h treatment. (B) Bacterial density and relative residual biofilm mass after 6-h treatment. (B) 3D images of biofilm after 6-h treatment observed by CLSM. Bacteria were stained with SYTO 9 and PI with live cells green and dead cells red.

Table 1. Size and surface characterization of CNCs and phages

	Particle size (nm)	**Zeta Potential (mV)**	**Surface N content (%)**	**Surface area (m^2/g)**
Fe_3O_4@APTES (S)	154 ± 16	+15.7 ± 0.3	2.87 ± 0.05	44.78 ± 0.98
Fe_3O_4@APTES (M)	256 ± 28	+14.1 ± 0.4	2.81 ± 0.06	38.48 ± 0.93
Fe_3O_4@APTES (L)	498 ± 34	+10.2 ± 0.3	2.01 ± 0.04	20.74 ± 0.96
Phage PEB1	54 ± 4	-17.3 ± 0.2	NA	NA
Phage PEB2	86 ± 4	-18.2 ± 0.2	NA	NA

Table 2. Semi-empirical model parameters.

Symbol	**Definition**	**Values**	**Sources**
L_1	Width of simulated biofilm	50 μm	Assumed
L_2	Height of simulated biofilm	6 μm	Measured
α_E	Infection rate coefficient toward *E. coli*	0.60 min^{-1}	Eqn. S1
α_P	Infection rate coefficient toward *P. aeruginosa*	0.45 min^{-1}	Eqn. S1
λ_H	Horizontal diffusion rate coefficient	0.10 min^{-1}	Eqn. S2
λ_V	Vertical diffusion rate coefficient	0.1 - 0.17 min^{-1}	Eqn. 4
δ_H	Horizontal trapping rate coefficient	0.75 min^{-1}	Eqn. S3
δ_V	Vertical trapping rate coefficient	0 - 0.75 min^{-1}	Eqn. 5
F_λ	Diffusion facilitation coefficient	0 - 0.7	Eqn. S4
F_δ	Trapping facilitation coefficient	0 – 1.0	Eqn. S5
N_0	Initial phage number	304 PFU	Calibrated
Δt	Time step	1s	Literature [16]

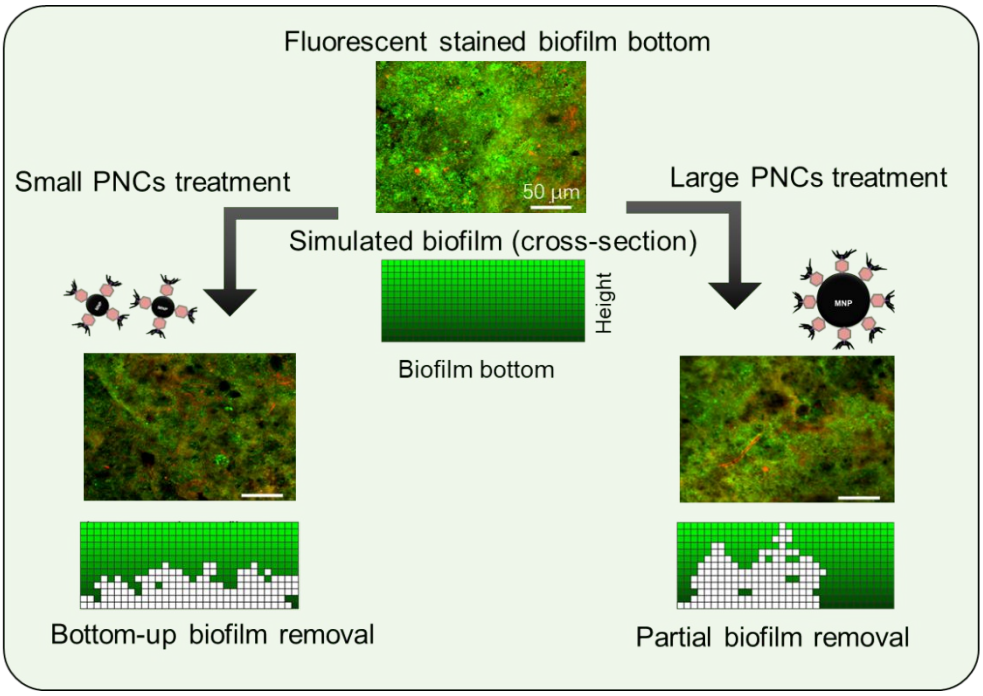

The combined experimental and computational study demonstrates an inverse relationship between phage-nanocomposite conjugates (PNCs) size and biofilm eradication potential.